Talanta 81 (2010) 1153–1161

Contents lists available at ScienceDirect

Talanta

journal homepage: www.elsevier.com/locate/talanta

An OEGylated thiol monolayer for the tethering of liposomes and the study of liposome interactions

Elisabeth Briand[a], Vincent Humblot[b], Claire-Marie Pradier[b], Bengt Kasemo[a], Sofia Svedhem[a,*]

[a] Chalmers University of Technology, Department of Applied Physics, 412 96 Göteborg, Sweden
[b] Laboratoire de Réactivité de Surface, UMR CNRS 7197, Université Pierre et Marie Curie, Paris 6, 4 place Jussieu, Case 178, 75252 Paris Cedex 05, France

ARTICLE INFO

Article history:
Received 29 September 2009
Received in revised form 12 January 2010
Accepted 17 January 2010
Available online 1 February 2010

Keywords:
Thiol-OEG SAM
Tethered liposomes
Melittin
Surface characterization
PM-RAIRS
XPS
QCM-D

ABSTRACT

The aim of the present work is to develop a protocol for the specific immobilization of liposomes, via tethers, onto functionalized gold surfaces, and in addition to give one example for such a surface architecture. All surface functionalization steps are charcerized and controlled. First, mixed thiolate self-assembled monolayers (SAMs) prepared from COOH- and OCH_3-terminated oligo(ethylene glycol) (OEG) alkane thiols were characterized by polarization modulation reflection absorption infrared spectroscopy (PM-RAIRS) and by X-ray photoemission spectroscopy (XPS). The composition of the mixed SAMs was found to be close to that of the thiol solution. Next, grafting of biotin conjugated with an NH_2-terminated OEG spacer (biotin–OEG–NH_2) to the COOH groups via conventional amine coupling was optimized with respect to the COOH/OCH_3 ratio of the SAM. The grafting of biotin–OEG–NH_2 was assessed by monitoring the binding of neutravidin and albumin to the biotinylated surfaces using quartz crystal microbalance with dissipation monitoring (QCM-D), as well as by PM-RAIRS. It was shown that a COOH/OCH_3 ratio of around 0.3 was sufficient to saturate the SAMs with neutravidin. Finally, tethering of liposomes onto the neutravidin-terminated SAMs, was achieved. As an application example, of a close packed layer of tethered liposomes was exposed to the membrane-penetrating peptide melittin. As monitored by QCM-D, the liposomes fused when interacting with the peptide and ruptured into an extended, supported lipid bilayer over the whole surface. In summary, the described surface modification has potential for the development of assays requiring tethered intact liposomes, or tethered planar bilayers. Such surface architectures are especially important for the study of transmembrane proteins and peptides.

1. Introduction

The study of transmembrane proteins is a major challenge in bio-related sciences. This class of proteins, crucial for the functioning of cells, is involved in various processes such as recognition events at the cell surface, structural transformations of the cell membrane, transmembrane transport and signal transduction. The function of these proteins is far from fully understood, to a large extent due to the difficulties to isolate them in their active form. In fact, they need a particular environment to adopt their correct conformation, in turn necessary for them to have the correct (native) function. In other words the transmembrane proteins need to be integrated in a system mimicking their natural environments, the cell membrane, such as a phospholipid bilayer separating two aqueous compartments. One way to achieve such architecture is to use tethered supported lipid bilayers (tSLB). The support can be of different chemical natures, and commonly silica [1], metals [2,3], or polymers [4] have been used. Metallic substrates allow the use of numerous sensitive and easy to handle surface-analytical techniques. In this work, gold has been chosen since it is versatile, not oxidized at atmospheric conditions, and not cyto-toxic. Several models of tSLB on gold have already been reported in the literature [5–17], and, among them, three main strategies can be identified: (i) decoupling the membrane from the support via thiolipids or analogs integrating a spacer [5–11], (ii) the use of a polymer cushion to support the lipid bilayer [12,13], and (iii) via proteins which are bond either to the underlying surface [14–16] or directly integrated into the membrane [17]. Each of these strategies has advantages and disadvantages, detailed in a recent review [18]. For instance, an atomically flat gold substrate is necessary to achieve good quality thiolipid layers [8], while polymeric and protein underlayers may induce steric hindrance of the aqueous compartment separating the membrane from the support.

In the present study, strategies (ii) and (iii) were combined. The polymeric underlayer was a functionalized self-assembled thiol monolayer (SAM) [19–22], onto which oligo(ethylene glycol) (OEG) derivatized biotin was grafted (Fig. 1). The biotin-functionalized surface allowed for the subsequent controlled binding of a protein,

* Corresponding author. Tel.: +46 31 772 1000; fax: +46 31 772 3134.
E-mail address: sofia.svedhem@chalmers.se (S. Svedhem).

0039-9140/$ – see front matter © 2010 Elsevier B.V. All rights reserved.
doi:10.1016/j.talanta.2010.01.027

neutravidin, and in the next step, specific tethering of biotinylated liposomes. By controlling the layer of adsorbed neutravidin, the space available under the lipid layers can be optimized, and by using OEG-containing thiols and spacers, a hydrated underlayer can be created such that the amount of non-specifically bound material can be reduced. We have chosen to combine long alkyl chains to form a dense and stable SAM, with the use of long enough OEG chains to allow an efficient hydration layer. The stepwise build up of the functionalized surface allows the results from this study to be applied to other chemical modifications.

The described surface modification steps were characterized by, three surface-sensitive analytical techniques; polarization modulated reflection absorption infrared spectroscopy (PM-RAIRS), which is sensitive to chemical bonds and their orientation with respect to the support, X-ray photoelectron spectroscopy (XPS), analyzing the atomic composition of the surface modification, and the quartz crystal microbalance with dissipation monitoring (QCM-D), measuring changes in mass (including associated liquid) bound to the surfaces. Finally, we present an example where the action of the toxin melittin on tethered liposomes was analyzed. The transmembrane peptide melittin is known to induce membrane rupture of liposomes [23] and upon acting on the tethered liposomes, a structure was formed which had the QCM-D characteristics of a supported lipid bilayer.

2. Materials and methods

2.1. Chemicals

The methoxy- and carboxylic acid-terminated thiols used in this work were obtained from PolyPure (Oslo, Norway) and have the following structures: $HS–(CH_2)_{10}–CO–NH–(CH_2)_2–(O–CH_2–CH_2)_{10}–O–CH_3$ (Compound **1**, shown the thiolate form in Fig. 1) and $HS–(CH_2)_{10}–CO–NH–(CH_2)_2–(O–CH_2–CH_2)_{11}–O–CH_2–CH_2–COOH$ (Compound **2**, shown the thiolate form in Fig. 1). Neutravidin was purchased from Pierce. *N*-(3-Dimethylaminopropyl)-*N*′-ethylcarbodiimide (EDC), *N*-hydroxysuccinimide (NHS), *O*-(2-aminoethyl)-*O*′-[2-(biotinylamino)ethyl]octaethylene glycol (biotin–OEG–NH_2), bovine serum albumin (BSA), melittin from bee venom, ethanolamine, and tablets for the preparation of phosphate buffered saline (10 mM PBS, pH 7.4) were from Sigma–Aldrich. L-α-Phosphatidylcholine from egg (egg-PC) and 1,2-dioleoyl-*sn*-glycero-3-phosphoethanolamine (DOPE) were from Avanti Polar Lipids and Sigma–Aldrich, and 1,2-dioleoyl-*sn*-glycero-3-phosphoethanolamine-*N*-(cap biotinyl) (biotin-cap-DOPE) were from Avanti Polar Lipids. Water was purified with a milliQ system (Millipore, resistivity > 18 MΩ cm^{-1}) and analytical grade ethanol was used.

2.2. Substrates

For PM-RAIRS and XPS measurements, Si wafers were coated with a 2 nm layer of Ti and a 200 nm layer of Au by e-beam evaporation using an AVAC 600, at a rate of 1 Å/s and a pressure of 5.10^{-6} mbar. The coated wafers were cut into squares of 1 cm × 1 cm. For QCM-D experiments, commercially available Au-coated crystals were used (Q-Sense AB, Sweden).

2.3. Protocol

Prior to use, all substrates were cleaned in a mixture of H_2O/NH_3 (25%)/H_2O_2 30% in a proportion of 5/1/1 at 70 °C for 10 min, after which they were thoroughly rinsed with water and dried under a stream of N_2. The successive functionalization steps are depicted in Fig. 1. First, gold-coated substrates were immersed for at least 18 h in a 1 mM thiol solution, with mixtures of the COOH- and OCH_3-terminated thiols in different ratios (Fig. 1-i). The compositions are referred to the proportion of the COOH-terminated thiol in solution (χ_{COOH}), and the series of tested χ_{COOH} fractions was 0, 0.01, 0.05, 0.1, 0.25, 0.5, 0.75 and 1. After incubation, the substrates were extensively rinsed with ethanol and dried under a stream of N_2. Next, after activation of the COOH-terminated thiols by the chemical reaction involving EDC (30 mM) and NHS (60 mM) in water [24] (Fig. 1-ii), a biotin–OEG–NH_2 solution, 1 mg/mL in PBS, was deposited on the top of the surfaces for 2 h (Fig. 1-iii). The surfaces were then in contact with ethanolamine, 1 M in water, to inactivate remaining succinimide ester groups. Solutions of BSA (100 mg/L) or neutravidin (40 mg/L) in PBS were used to test non-specific and specific interactions with proteins, respectively. The specific binding of liposomes was then assayed using liposomes prepared by a lipid mixture (egg-PC/DOPE 60/40 w/w) with or without biotinylated lipid (2% w/w) added to it. The liposomes were prepared by

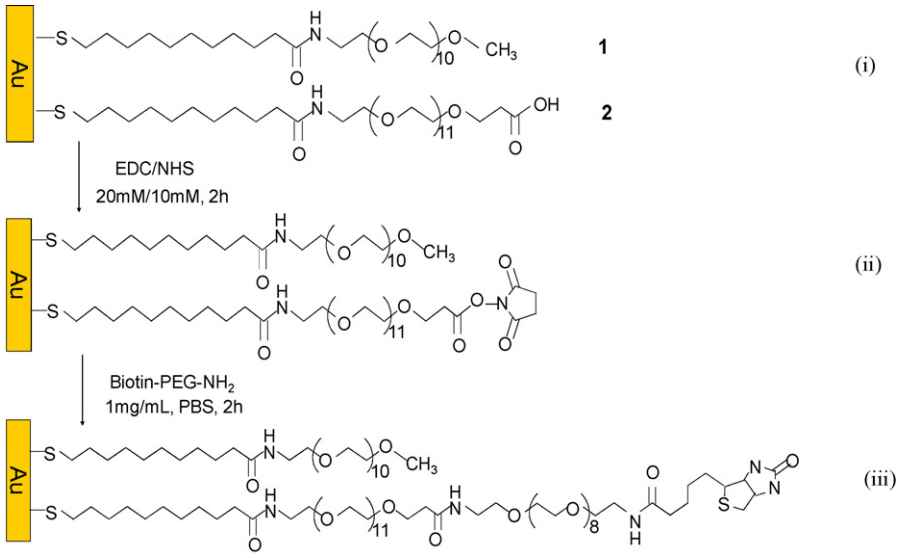

Fig. 1. Reaction scheme for the series of reactions carried out on gold-coated surfaces. (i) OEG–thiolate SAM prepared in an incubation solution where the proportion of the two thiols **1** and **2** is given by χ_{COOH}; (ii) SAM where the COOH-terminated thiolates have been transformed into active esters by NHS/EDC; (iii) SAM where biotin–OEG–NH_2 has been coupled covalently (this step is followed by deactivation by ethanolamine).

(i) dissolution of the lipids in chloroform, (ii) drying of the film by evaporation of the solvent first under a stream of N_2, then under vacuum for at least 2 h, (iii) re-suspension of the lipid film in PBS buffer to obtain a stock solution of 5 mg/mL, and (iv) extrusion (using the Avanti Polar Lipids mini-extruder) of the solution 11 times through two membranes, first with pores of 100 nm and then with pores of 30 nm. Liposomes prepared in this way will typically get a size of 90 nm [25].

2.4. Measurements

2.4.1. PM-RAIRS measurements

The FT-IR instrument used was a NICOLET Nexus 5700 FT-IR spectrometer. The external beam was focused on the sample with a mirror, at an optimal incident angle of 85°. A ZnSe grid polarizer and a ZnSe photoelastic modulator, modulating the incident beam between p and s polarizations (HINDS Instruments, PEM 90, modulation frequency = 36 kHz), were placed prior to the sample. The light reflected at the sample was then focused on a N_2-cooled MCT detector. The sum and difference interferograms were processed and Fourier-transformed to yield the differential reflectivity $\Delta R/R = (Rp - Rs)/(Rp + Rs)$ which is the PM-RAIRS signal. 100 scans were recorded at 8 cm^{-1} resolution for each spectrum. The measurements were done at two different voltages applied to the modulator ZnSe crystal for an optimized PM-RAIRS sensitivity.

2.4.2. XPS measurements

The XPS analyses were performed using a PHOIBOS 100 X-ray photoelectron spectrometer from SPECS GmbH (Berlin, Germany) with the Mg Ka X-ray source ($h\nu$ = 1253.6 eV) operating at 1×10^{-10} Torr or less. Spectra were recorded with a 20 eV pass energy for the survey scan and 10 eV pass energy for the C1s, O1s, N1s, S2p and Au4f regions. High resolution XPS conditions have been fixed, "Fixed Analyser Transmission" analyses mode, a 7 mm × 20 mm entrance slit and 150 W electron beam power (12.5 kV and 12 mA). A takeoff angle of 90° from the surface was employed for each sample and binding energies were calibrated against the $Au4f_{7/2}$ binding energy at 84.0 eV. Element peak intensities were corrected by Scofield factors [26], the spectra were fitted using Casa XPS v.2.3.13 Software (Casa Software Ltd., UK) and applying a Gaussian/Lorentzian ratio, G/L equal to 70/30.

2.4.3. QCM-D measurements

The QCM-D measurements were made in the liquid phase using two different QCM-D systems (QCM-D E4 and QCM-D 300, Q-sense AB, Sweden), which allow for real-time monitoring of both the resonance frequency, f, of the quartz crystal and the dissipation, D, resulting from damping of the oscillation due to the added overlayers. Frequency shifts, Δf, are related to changes in mass adsorbed on the sensor surface, whereas dissipation shifts, ΔD, are related to the structural and viscoelastic properties of the layer adsorbed on the sensor surface [27,28]. The liquid cell was either connected to a peristaltic pump, and the flow rate was 100 μL/min (in experiments performed with QCM-D E4), or operated in batch mode (with QCM-D 300 – total cell volume: 100 μL). Frequency shifts Δf_n, measured at overtone n, were renormalized to the fundamental frequency value by dividing Δf_n by n.

3. Results

The data obtained during the stepwise functionalization of the gold substrates are organized and presented in the following way. First the preparation of the alkane thiolate OEG-SAMs and the activation of exposed COOH groups, characterized by PM-RAIRS and XPS, are described. Then follow the grafting of the biotin moieties to the activated SAMs and the subsequent biospecific binding of neutravidin characterized by PM-RAIRS and QCM-D. Finally the tethering of biotinylated liposomes to the neutravidin-modified surfaces, measured by QCM-D, is described. In the last part, an application example is given, where melittin is allowed to interact with tethered liposomes.

3.1. Characterization of the SAMs

In the first preparative step, the SH moieties of the OEG-containing thiols react spontaneously with gold to form a strong bond between gold and the corresponding thiolate. This results in the formation of a SAM at the gold/ethanol interface. Pure and mixed monolayers of thiolates **1** and **2** (Fig. 1) were formed and characterized by PM-RAIRS and XPS.

3.1.1. PM-RAIRS results

Fig. 2 shows the PM-RAIRS spectra of the gold surface modified by a SAM of CH_3O–OEG–thiolate **1** (spectra c) and COOH–OEG–thiolate **2** (spectra a). Two spectral regions have been probed, corresponding to the methylene stretching region at 2800–3000 cm^{-1} (Fig. 2A) and to the fingerprint region at 1000–2000 cm^{-1} (Fig. 2B).

The spectra at high frequencies (Fig. 2A) show specific features of the CH_2 symmetric and asymmetric stretching bands of methylene groups in the hydrocarbon chains at 2854 cm^{-1} and 2919 cm^{-1}, respectively, the asymmetric stretching band of CH_3 in the methoxy group at 2958 cm^{-1}, and a band corresponding to CH_2-stretching vibrations of the EG repeats at ca. 2865 cm^{-1}. In the 2000–1000 cm^{-1} region, one can observe the characteristic vibrations of OEG chains both in the amorphous and the crystalline states: the IR bands correspond to the ether CH_2 wagging (1355 cm^{-1}) and twisting (1290 cm^{-1}) vibrations and the COC

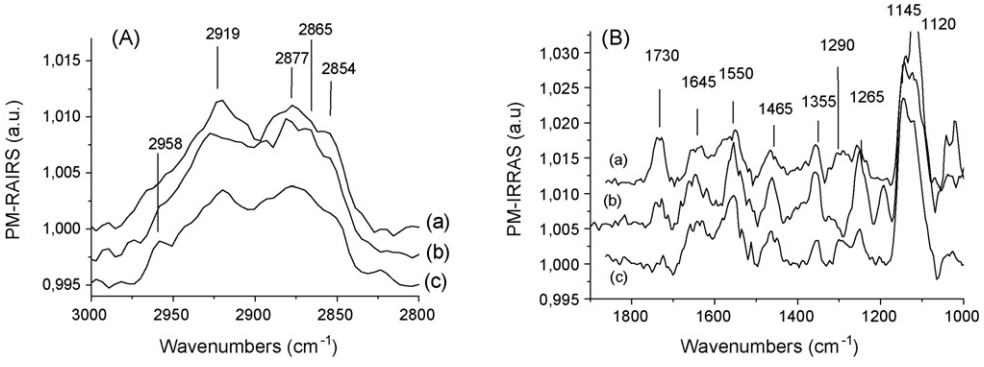

Fig. 2. (A) The CH_2-stretching region and (B) the 1000–2000 cm^{-1} region of PM-RAIRS spectra of SAMs prepared from (a) the COOH-terminated thiol **2** and (c) the OCH_3-terminated thiol **1**. The spectra (b) correspond to a mixed SAM with a χ_{COOH} of 0.25.

stretching band (1145 cm^{-1}) for OEG chains in an amorphous state [3,29,30]. The presence of a second peak at 1120 cm^{-1} (COC stretching) and 1265 cm^{-1} (ether CH_2 twisting) indicates the presence of OEG chains in a helical configuration. The latter band may include the contribution of the amide III band. The amide bond between the mercaptoundecanoic acid and the OEG moieties are clearly observable through the amide I (1645 cm^{-1}) and amide II (1550 cm^{-1}) bands, corresponding to the C=O stretching, and to the N–H bending coupled with the C–N stretching, respectively. The last band, at 1730 cm^{-1}, corresponds to the C=O stretching of COOH-terminated thiolate **2**, and is only seen on surfaces with acidic thiolated molecules.

Some IR features cannot be assigned to only one given molecule. This is the case of the amide I and amide II bands, which are present in both kinds of thiols adsorbed at the surface. We do not see a variation in the relative height of these two bands (features present at 1645 cm^{-1} and 1550 cm^{-1} on all spectra of Fig. 2), which could be the case if the orientation of the layer was modified between different surfaces. Then, we can calculate the integrated intensity of these bands for the various mixed SAMs (χ = 0, 0.1, 0.25, 0.5, 0.75, 1). It was found to be, in all cases, between 0.75 a.u. and 1 a.u., without any specific trends. These variations are in the range of the experimental uncertainty. Thus the formation of monolayer from mixture of thiols does not induce a net modification in the layer density.

The correlation between the ratio of the two thiols in solution and the composition of the SAMs could be investigated by considering the area of $\nu_{C=O}$ band in COOH moieties (1730 cm^{-1}). However, the likely presence of COO^- groups at that step – whose vibrations are not well resolved in the IR spectra and thus cannot be used to determine the ratio of carboxyl moieties on the surface – could lead to a misinterpretation in the analyses of the IR intensity. To overcome this potential problem, bands appearing at the next step, after formation of succinimide ester (Fig. 1-ii), were considered. The carboxylic acid groups react with NHS, via a reaction catalyzed with the EDC, to form reactive succinimide ester groups (Fig. 1-ii), whose IR signature consists of three bands, at 1745 cm^{-1}, 1790 cm^{-1} and 1820 cm^{-1}. The series of spectra is reported in Fig. 3. Three IR bands appear after the esterification: a main band at 1745 cm^{-1}, assigned to the $\nu_{C=O}$ of the ester groups, and two less pronounced bands, at 1790 cm^{-1} and 1820 cm^{-1} corresponding to the $\nu_{C=O}$ vibrations of the succinimide group [24,29,31]. The intensity of the band at 1745 cm^{-1} is proportional to the quantity of ester groups on the surface. They are reported in the inset of Fig. 3.

The ester band intensity increases linearly with the fraction of COOH-terminated thiol in solution, with a slight decrease of the slope at the highest fraction of COOH groups. The uncertainty of the measure does not allow us to give further interpretation about this possible effect. All these IR assignments are summarized in Table 1.

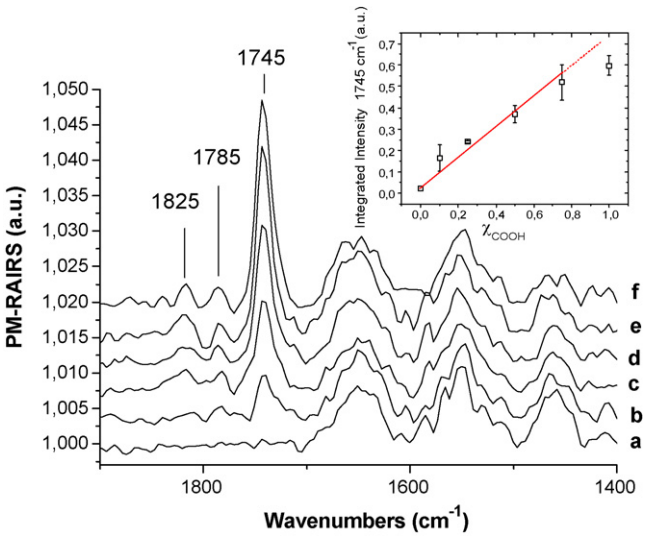

Fig. 3. PM-RAIRS spectra after activation by NHS and EDC for different fractions of the COOH-terminated thiol **2** in solution (series of χ_{COOH}: 0, 0.1, 0.25, 0.50, 0.75, 1). Inset: intensity of the 1745 cm^{-1} band in Fig. 4 for the different χ_{COOH}. The fit of the data according to a linear equation is also presented and is performed on all data excepted χ_{COOH} = 1. The dashed line corresponds to the extrapolation of this fitting line.

3.1.2. XPS results

The different SAMs were further characterized by XPS to determine the surface concentration of the various elements. The C1s and O1s spectra were recorded for different compositions of the SAMs. The spectra obtained for a SAM of the COOH-terminated thiolate **2** (χ = 1) are presented in Fig. 4. The two signals were decomposed into several contributions, in very good agreement with the chemical groups present in the molecules.

The C1s spectrum was dominated by the contribution at 286.8 eV from carbon in the C–O–C bonds of the OEG chains. The contribution of the C–C and C–H bonds is at lower binding energy, at 284.9 eV. A small contribution from carbons at high energy, 289.1 eV, which is characteristic for carbon atoms involved in COOH groups, was also distinguished. We attribute this unexpected contribution to the presence of a small contamination of unreacted mercaptoundecanoic acid, remaining from the synthesis of the compounds, in all thiol solutions, including that of the methoxy-

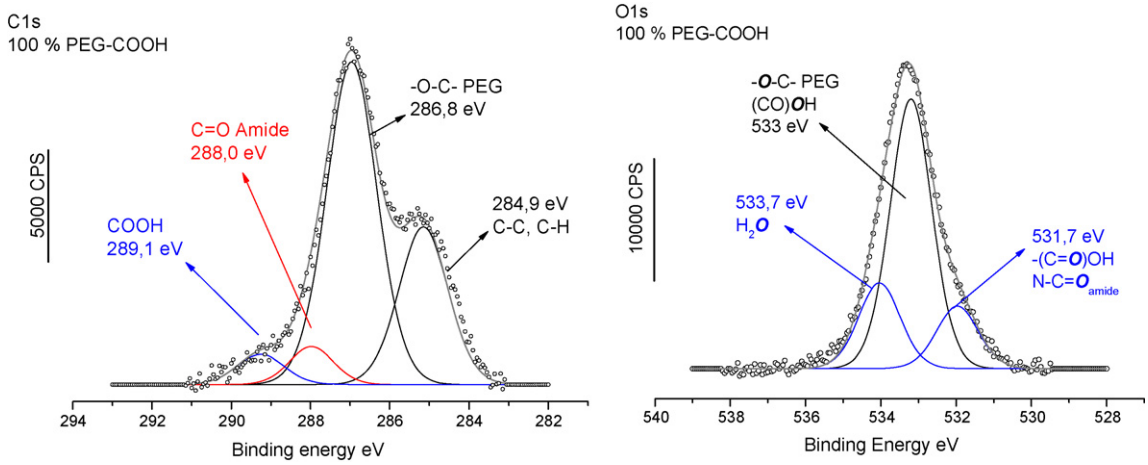

Fig. 4. C1s and O1s spectra obtained from SAM of thiolate **2** (χ_{COOH} = 1). The decomposition of the signals is described in the figure.

Table 1
Summary of the IR band assignments in the IR spectra of the two pure SAMs [3,29,30].

Wavenumber (cm^{-1})	Assignment
1120	ν_{COC} (crystalline structure)
1145	ν_{COC} (amorphous layer)
1265	$\delta_{Ether\,CH_2}$ (crystalline structure) amide III (δ_{NH} and ν_{C-N})
1290	$\delta_{Ether\,CH_2}$ (amorphous layer), ν_{C-O} in COOH (1280)
1355	$\omega_{Ether\,CH_2}$ (amorphous layer)
1465	$\delta_{Ether\,CH_2}$-(scissoring) $\nu_{symCOO-}$ (1400–1430 cm^{-1})
1550	amide II, δ_{NH} coupled with ν_{C-N}
1590	$\nu_{asym\,COO}$
1645	amide I, $\nu_{C=O}$ in R-CONH-PEG
1730	$\nu_{C=O}$ in COOH
2854	ν_{sCH_2} in hydrocarbon chains
2865	ν_{sCH_2} in PEG chains
2919	ν_{asCH_2} in hydrocarbon chains
2945	ν_{asCH_2} in PEG chains
2958	ν_{asCH_3}

terminated thiol **1**. In the rest of the study, a contribution equal to that observed on the pure methoxy-terminated thiolate SAM, has been substracted from the C1s peak for the calculation. Finally, the component at 288 eV has been attributed to carbon atoms involved in amide bonds.

Similarly to the C1s signal, the O1s signal was decomposed in several contributions depending on the chemical environment of the atoms. The component at high binding energy, 533.7 eV, is attributed to oxygen atoms present in water trapped into the layer, the contribution at 533 eV corresponds to the O1s signal of atoms linked to hydrogen or carbon by a single bond, and the contribution at lower binding energy, 531.7 eV, is characteristic of oxygen involved in a C=O bond (COOH and CONH).

The intensities of the C1s and O1s components at 289.1 eV and 531.7 eV were used to calculate the fraction of the COOH-terminated thiolate **2** in the mixed SAMs. The results are displayed in Fig. 5, where a linear increase of this contribution versus the proportion of the COOH-terminated thiol in solution can be observed. For both signals, the increases correlate nicely with the expected ones, thus confirming that the ratio of COOH- and CH_3O-terminated thiolates on the surface is nearly identical to the corresponding ratio between the thiols in solution.

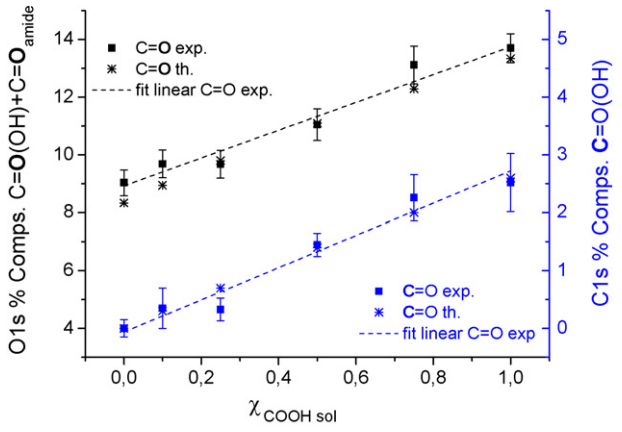

Fig. 5. Percentage of the contribution of the component at high energy in the total C1s (□) and O1s (■) signal versus χ_{COOH} in solution. These data have been compared to the one obtained in an ideal SAM, respectively, for the C1s (*) and O1s (*). Linear fit of the data is presented as dashed lines. The ideal SAM is one whose thiol composition on the surface reflects exactly the proportion of thiol in solution. The contribution of the COOH contamination has not been removed from the O1s signal and thus explains the slight differences between C1s and O1s results.

The thickness d of the SAMs can be estimated by XPS from the attenuation of the gold signal, according to the relation:

$$\frac{I_{Au4f}}{I^0_{Au4f}} = e^{d/\lambda} \quad (1)$$

where I_{Au4f} is the intensity of the $Au4f_{7/2}$ signal of the sample, I^0_{Au4f} the intensity of the $Au4f_{7/2}$ signal for a bare surface, and λ the mean free path of the gold 4f electrons through a dense organic layer taken to be equal to 35 Å in the present experiment [32].

The thicknesses of the mixed SAMs as determined by XPS were between 25 Å and 29 Å. The observed differences are of the order of the uncertainty of the measure. This thickness is higher than the one recorded for a pure mercaptoundecanoic acid SAM (14 Å) [33], but lower than that of expected if the OEG–thiolate molecules were fully extended or presenting only helical structures (43 Å) [34,35]. This supports the interpretation of the IR data that the major part of OEG chains is in amorphous state in the SAM.

3.2. Grafting of biotin to activated SAMs and biospecific binding of neutravidin

In order to biospecifically bind neutravidin, and subsequently liposomes, on the OEG-thiol-functionalized surfaces, biotin molecules, modified with aminoOEG groups, were grafted to the activated SAMs (Fig. 1-iii).

3.2.1. PM-RAIRS results

The series of IR spectra in Fig. 6 demonstrates how it was possible to follow in detail the different steps during the functionalization of a COOH-terminated SAM ($\chi_{COOH} = 1$). The spectra

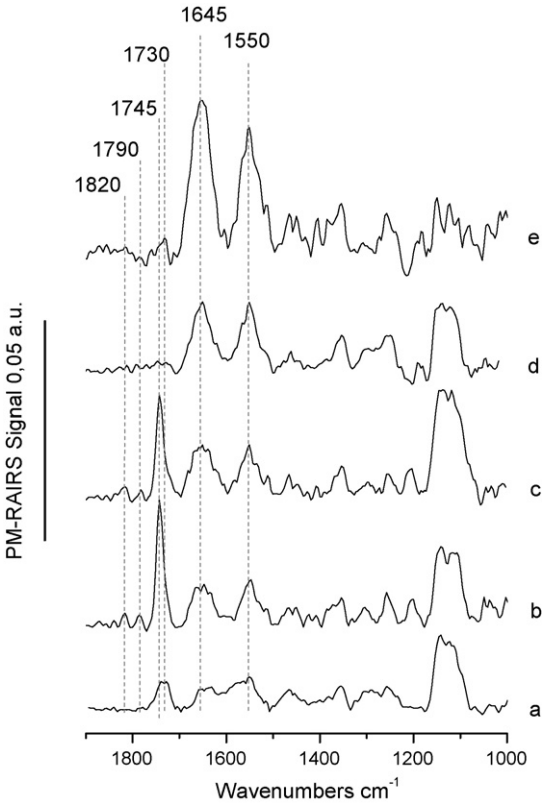

Fig. 6. PM-RAIRS spectra of a SAM of the COOH-terminated thiolate **2** recorded after (a) assembling of the SAM, (b) formation of succinimide ester after reaction of the carboxylic moieties with NHS and EDC, (c) grafting of biotin–OEG–NH_2, (d) reaction of the remaining reactive ester group with ethanolamine, and (e) biospecific binding of the neutravidin.

correspond to (a) the SAM as assembled, (b) after activation by NHS and EDC, (c) after grafting of biotin–OEG–NH_2, (d) after deactivation of the remaining succinimide esters at the surface, and finally (e) after binding of neutravidin.

The 1745 cm^{-1} band vanishes upon the reaction of the succinimide ester with the NH_2 moieties of biotin–OEG–NH_2 (Fig. 6c), followed by contact with ethanolamine (Fig. 6d) or hydrolysis, resulting in the appearance of additional amide bonds. The IR spectrum recorded after reaction of the succinimide esters with biotin–OEG–NH_2 (Fig. 6c) displays slight differences compared to the one recorded after activation of the carboxylic acid group (Fig. 6b). All spectra show similar results for mixed SAMs. One can see a small decrease of the ester $\nu_{C=O}$ band at 1745 cm^{-1}, suggesting a consumption of these functionalities, along with a slight increase of both amide I and amide II and ν_{C-O-C} bands, respectively, present at 1645 cm^{-1}, 1550 cm^{-1} and ~1140 cm^{-1}, clearly suggesting the successful grafting of a small quantity of biotin conjugates. The amount of biotin grafted is very low compared to the number of activated COOH groups, and we cannot discriminate between the different SAMs at this step. The reaction of the remaining succinimide ester groups with ethanolamine is quantitative since no ester bands are seen after the deactivation step (Fig. 6d).

One can readily follow the grafting or binding of proteins through the evolution of the bands corresponding to the amide bonds (mainly amide I and amide II, at 1650 cm^{-1} and 1540 cm^{-1}, respectively – Fig. 6e). Before investigating the specific binding of neutravidin on surfaces, non-specific physisorption of proteins on the layers was tested by the admission of BSA, commonly used for such tests. The amount of adsorbed BSA, measured both by PM-IRRAS and QCM-D, is negligible on all surfaces (data not shown), meaning that the surfaces present a good resistance to non-specific protein adsorption. In addition, the binding of neutravidin to the biotinylated surfaces is apparent from the increase in intensity of the amide I (1645 cm^{-1}) and amide II (1550 cm^{-1}) bands

3.2.2. QCM-D results

The QCM-D results are presented together with PM-RAIRS to facilitate the comparison between results obtained in air and in liquid.

Fig. 7 displays the increase of the amide I and amide II band intensity and the QCM-D frequency shifts recorded after neutravidin binding. An example of the *f* and *D* signals recorded by QCM-D are reported in Fig. 8. The low level of dissipation (0.6×10^{-6}) indicates the formation of a rigid protein layer on the top of the substrate.

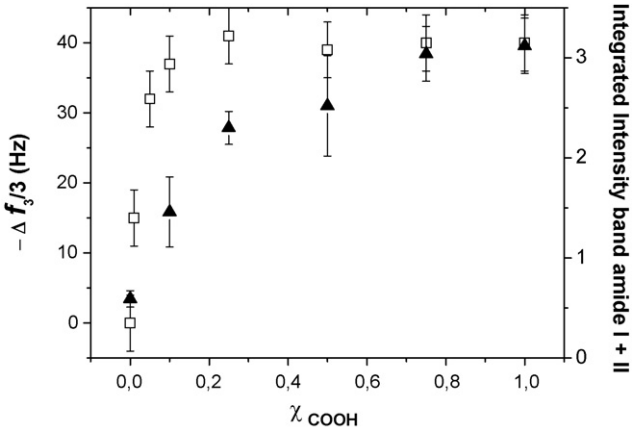

Fig. 7. Normalized frequency shifts (□) and amide I and amide II band areas (▲) recorded after binding of neutravidin on SAMs with different χ_{COOH}. These data are an average of two sets of measurements.

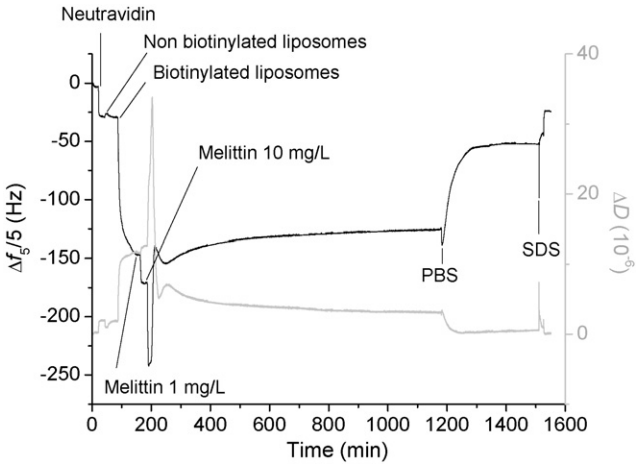

Fig. 8. Normalized frequency (black) and dissipation (grey) shifts recorded on a surface functionalized with a χ_{COOH} of 0.1 SAM, biotin-OEG-NH2 when neutravidin, non biotinylated liposomes, biotinylated liposomes and melittin are introduced in the measuring QCM-D chamber.

From Fig. 7 it is obvious that the amount of adsorbed protein increases with the proportion of COOH-terminated thiols in the layer, until saturation of the surface occurs. The saturation level in the QCM-D data corresponds to the expected value for a full monolayer coverage of protein [36], indicating that the proportion of COOH moieties in the SAM necessary to fully cover the surface in neutravidin is around 30–40%. A slight difference appears upon comparison of QCM-D and PM-RAIRS data, likely due to different surface treatments before the analyses (drying or not drying the surfaces for instance).

3.3. Tethering of liposomes to the biotinylated SAMs

The tethering of liposomes as monitored by QCM-D alone, since this step requires working in a liquid environment. The presence of neutravidin on the surface allows for specific tethering of liposomes, which expose biotin moieties at their surface. To test the specificity of the liposome immobilization, experiments were also done with a suspension of liposomes with the same lipid composition but without biotinylated lipids. The normalized frequency shifts recorded after stabilization of signals are reported in Table 2.

The level of non-specific binding of liposomes is low, apparently because the underlying cushion of OEG helps to prevent liposome adsorption, even when the surface coverage of neutravidin is incomplete. Nevertheless we note that the non-specific binding level is a little higher on surfaces with a low coverage of neutravidin ($\chi_{COOH} < 0.3$) compared to when full protein coverage is achieved, suggesting that the passivating effect of these OEG-thiols is not perfect. A second observation concerns the amount of specifically

Table 2
Frequency shifts recorded after adsorption of neutravidin, non specific- and specific-binding of liposomes. The experiments were made several times on two kinds of apparatus. The uncertainty of the value is estimated to be 10% of the signal and is mainly due to the amount of water trapped in the liposomes, which can vary a little from one extrusion to another.

$\chi_{(COOH)sol}$	Neutravidin	Non biotinylated liposomes	Biotinylated liposomes
0.01	16 Hz	7 Hz	110 Hz
0.05	32 Hz	9 Hz	105 Hz
0.1	37 Hz	6 Hz	100 Hz
0.25	40 Hz	3 Hz	110 Hz
0.5	39 Hz	2 Hz	120 Hz
0.75	40 Hz	1 Hz	125 Hz
1	40 Hz	1 Hz	117 Hz

tethered liposomes (Table 2), which obviously does not increase significantly with the amount of neutravidin. The amount of neutravidin, for $\chi_{COOH} = 0.25$, is twice that on SAMs with $\chi_{COOH} = 0.01$, while the amount of tethered liposomes is the same on those two surfaces. This can be explained by the difference in sizes between neutravidin and the liposomes; the former is close to 5 nm, while liposomes have a diameter of about 90 nm. It is thus not surprising that the liposomes cover several neutravidin molecules even if the protein layer is incomplete.

3.4. Application example: interaction of tethered liposomes with melittin

As an application example of the developed surface modification protocol, tethered liposomes were allowed to react with a pore-forming peptide, the toxin melittin from bee venom. The experiment was monitored by QCM-D. The sensor surface was functionalized by a mixed SAM with a $\chi_{COOH} = 0.1$. The QCM-D responses, Δf and ΔD, during the sequential interactions of biotintylated SAM with non-biotinylated liposomes, biotinylated liposome, melittin (first at a low concentration, and then at a higher concentration), and detergent (SDS) are shown in Fig. 8. The interaction of tethered liposomes with melittin was tested several times, and showed reproducible results. At a low toxin concentration (1 mg/ml), the frequency decreased (corresponding to mass uptake) and the dissipation increased (corresponding to a less rigid structure) to reach stable levels at ($\Delta f \sim -20$ Hz and $\Delta D \sim 1 \times 10^6$). When a higher melittin concentration (10 mg/L) was used, more complex features were observed. The frequency shift descreased sharply (mass uptake), until it reached a minimum ($\Delta f \sim -70$ Hz), and then increased again to reach a value similar to the one observed directly after tethering of the liposomes. Similarly, the dissipation signal was drastically affected, increasing first up to $\Delta D \sim 32 \times 10^6$ before drastically decreasing and stabilizing at $\Delta D \sim 3 \times 10^6$. A rinsing step with buffer induced an additional increase in the frequency shift (mass loss) before stabilization of the signal. The difference in the frequency shift observed between the signal after immobilization of the neutravidin ($\Delta f \sim -26$ Hz) and after rinsing with PBS ($\Delta f \sim 53$ Hz) was -27 Hz. The value of the dissipation at this point corresponded to $\Delta D \sim 0.4 \times 10^6$. These values are representative for planar supported bilayers with few defects. The tethered membrane could be removed by a pulse of detergent.

4. Discussion

Two surface characterization techniques (PM-RAIRS and XPS) were used to study the surface composition and the order of mixed SAMs formed from OEGylated thiols presenting long alkyl chain lengths and two different head groups (COOH and OCH_3). The aim of the study was to investigate the influence of the monolayer composition on the reactivity of the surfaces, and to show their applicability to the study of supported lipid membrane structures (liposomes and bilayers)

4.1. Relation between structural and functional properties of the SAM

The PM-RAIRS results show the characteristic wavenumbers (ν_{asCH2} at 2919 cm^{-1}) for a well-organized and densely packed hydrocarbon chains in the all-trans configuration [37,38]. We have thus achieved a good crystallinity of the C11 alkyl chains in the SAM. Similar structures have been observed for the same kind of compounds by others [30], and the order of the layer was improved by the stabilizing effect of the H-bond in the amide group.

The spectral features corresponding to the OEG moieties of the molecules in the SAM exhibit wavenumbers indicating the coexistence of amorphous and helical structures. This is confirmed by the XPS results, where the calculated thickness of the layer is lower than that expected for a SAM composed of fully extended molecules. A larger fraction of OEG chains in the helical conformation has been observed for similar SAMs on gold, and the helical structure was shown to be facilitated by a number of ethylene glycol unit higher than 6, but also to be temperature-dependent [30]. Analogous thiols with an ether bond instead of the amide bond between the alkyl chain and the OEG moiety have been shown to adopt different structures depending on the substrate [3]. On gold, the OEG chains will adopt a helical conformation, whereas on silver, an all-trans configuration is observed. It has been suggested that the helical and amorphous conformations are more suitable to resist non-specific protein adsorption [34].

XPS and PM-RAIRS results show that coadsorption from a solution containing the two thiol species leads to a composition of the SAM very close to that in solution. This result is expected, after using OEGylated thiols having the same alkyl chain lengths, although small differences between the thiols can be enough to induce phase segregation and preferential adsorption of one of the thiols in solutions [39,40].

The reactivity of the terminal COOH groups exposed by the SAMs was good. It was shown by PM-RAIRS how the COOH groups were successfully transformed into succinimide esters. The complete removal of the characteristic absorption band at 1730 cm^{-1} allows us to suppose that the reaction was quantitative, or very close to quantitative. In contrast, the grafting of biotin–OEG–NH_2 molecules to the activated SAM did not induce drastic changes in the IR spectra, meaning that, for all SAMs, only a part of the ester groups reacted with the biotin. This was a very likely outcome due to the disordered structure of the OEG functionalities (amorphous part of the layer): it "may hide" some of the reactive esters inside the layer, which makes them not easily accessible for the biotin–NH_2 molecules, due to the high exclusion volume of the hydrated OEG layer. This limitation does not occur during the reaction with ethanolamine, likely due to the high concentration of the compounds and its small size. Another factor that could be involved in the difference in grafting efficiency between biotin–NH_2 and ethanolamine is the solvent. In the former case, it is a saline buffer while in the later one, only water is used. It is well known that the presence of salt modifies the structures of the OEG chains, which can vary between mushroom- and brush-shaped layers depending on the salt concentration. A similar effect for the OEG could explain the better accessibility to the ester groups.

4.2. Grafting of biotin–OEG–NH_2 and biospecific binding of neutravidin

The biotinylated SAMs allow for the specific binding of neutravidin (BSA only adsorbed in small quantities), confirming the grafting of the SAM with biotin moieties. Moreover, the amount of biospecifically bound neutravidin is dependent on the proportion of COOH groups in the SAM. We observed by two techniques, PM-RAIRS and QCM-D, a saturation of the surface with respect to binding of neutravidin for a value of χ_{COOH} of about 0.3. Apparently, from QCM-D data, a lower χ_{COOH} (about 0.1) is needed to reach saturation than observed by PM-RAIRS. This slight discrepancy is likely due to the difference in the experimental conditions; the rinsing with water followed by drying of surfaces during the preparation of the samples for PM-RAIRS may induce partial removal of neutravidin, which could explain the higher level of neutravidin required to saturate the surfaces. Whatever the technique, the main result is that only a small fraction of a biotin monolayer at the surface is necessary to achieve a full coverage of neutravidin.

This is in agreement with previous studies, in which a fraction of 0.05–0.1 was needed to reach a full coverage of protein [41–43]. However, we do not observe a decrease in the amount of bound proteins to the surface at higher χ_{COOH}, previously observed by others [41,42]. This observation was attributed to the close packing of the biotin moieties at high biotin fraction, which is outside the range of the present study, due to the relatively inefficient coupling reaction of the biotin–OEG–NH_2 molecules to the activated SAMs.

For the type of surface preparation and studies described here, a good balance in the morphology of the OEG layer is important. A good crystallinity of the OEG moieties in an all-trans configuration should enhance the accessibility of the head groups by presenting them at the interface layer/buffer, and therefore increase their reactivities toward further chemical modification. However, this structure induces a loss in the degree of hydration of the layers and decreases their ability to repel non-specific protein adsorption [44]. In the present work, the reactivity of the layers toward the grafting of biotin was low, likely due to the high degree of disorder in the OEG layer. Nevertheless, the amount of bound biotin was high enough to allow a full coverage of biospecifically bound neutravidin.

4.3. Tethering of liposomes

Specific binding of biotinylated liposomes to the neutravidin-modified surfaces was successfully implemented. The amount of adsorbed vesicles was roughly the same on all surfaces, even on the surfaces not fully covered by neutravidin. It means that a full underlayer of proteins is not required to saturate the surface with liposomes, and this can be an advantage for the further formation of the tethered lipid bilayers, since steric hindrance of access to aqueous compartment will be reduced and more space may be available for transmembrane proteins.

4.4. Rearrangement of tethered supported structures upon interaction with melittin

As an example of the way the described surface modification can be used, the interaction of melittin with tethered liposomes was studied. Melittin is known to interact with membranes, and indeed complex and dynamic structural modifications of the tethered liposomes were induced by the action of melittin. The interaction of liposomes with melittin is initially accompanied with increases in mass and dissipation of the tethered lipid structures. The frequency and dissipation shifts observed are much too high to be explained solely by the adsorption of the peptide, but can instead be rationalized by interaction and fusion of neighboring liposomes under the action of melittin resulting in the formation of highly dissipative structures with more trapped water. A similar phenomenon has been observed under the action of a synthetic amphipathic alpha-helical peptide with POPC vesicles adsorbed on gold [45,46]. Another interesting feature is the sharp decrease in dissipation after a maximum has been reached, which stabilized at a lower level than after the initial immobilization of the liposomes. It means that whatever the resulting lipid structure is, it has undergone a stiffening, monitored as a reduced D and a change in viscoelastic properties. At the same time, after a temporary huge decrease, the frequency has regained approximately the same level as after the initial adsorption of liposomes. This suggests that the amount of lipid and trapped water (which will contribute much more to the frequency and dissipation signals than the toxin *per se*) has not changed very much after all the structural changes have been processed. After rinsing with buffer, the frequency increased and stabilized at a value about 27 Hz lower than that the one observed before liposome adsorption, and the dissipation was very low. These two values taken together are, based on the prior extensive work on supported lipid bilayer formation, a strong indication of formation of a planar lipid bilayer [Keller and Kasemo]. Cho and coworkers had reached this value without a rinsing step, while it is very likely that in our case, adsorbed material was remaining on the surface after bilayer formation. This can be explained by the fact that we switched off the pump during the experiment. Since melittin is also an amphipathic alpha-helical peptide, it is likely that the action of the toxin is similar to the one described by Cho and coworkers and that we have achieved the formation of tSLB on the top of the polymer layer.

In our work the tethered membrane is formed via specific adsorption of liposomes on the top of a polymer cushion that reduces the amount of non-specific interaction. More work is needed to gain a better insight on the structure of the membrane formed here. This should be done by using further complementary techniques such as fluorescence microscopy, reflectometry [46] and electrochemistry methods [47,48]. For example, the mechanism of liposome adsorption, spreading and rupture on Hg electrode has been investigated by chronoamperometry, which has enabled to discriminate between various adsorption/deformation scenarios [47]. It would be interesting to further analyze in time structural changes that could occur on the system presented here by this approach, complemented with impedance spectroscopy [48].

5. Conclusion

This work demonstrates the assembly of thiols consisting of a long-chain alkyl moiety and an OEG chain in mixed SAMs exposing different fractions of COOH groups on the surface, and the subsequent grafting of OEGylated biotin to these surfaces. It was shown that the grafting efficiency was relatively low, a price paid to reduce non-specific adsorption of neutravidin and/or liposomes in a later step, but enough to control the specific binding of neutravidin molecules on the surface up to a full surface coverage. All molecules were commercially available and could help to spread the use of polymeric SAM in biointerface development. The described SAM architecture combines two advantages: the formation of an hydrated underlayer resistant to non-specific adsorption of proteins and liposomes, and the controlled immobilization of proteins that allows specific adsorption of liposomes and the formation of an extra aqueous space between the liposomes and the surface. It was shown that a very low surface coverage of biotin is needed to achieve the specific binding of neutravidin and that only a fraction of a saturated monolayer of neutravidin on the surface is necessary to saturate the surface with biotinylated liposomes. These tethered layers of liposomes can be used, e.g., to screen for membrane rupturing agents, or inhibitors of lipases. It was shown how the tethered liposomes overlayer interacted with melittin. The latter induced, depending on the melittin concentration, either fusion of the liposomes to larger liposomes or, as judged from the QCM-D results, the formation of a tethered lipid bilayer on the top of the protein/polymer surface modification.

Acknowledgments

Authors want to thank Dr. Christophe Méthiver of the Laboratoire de Reactivité de Surface (Paris) for his help with XPS measurements. The SSF (Swedish Foundation for Strategic Research) Biomics Program, VINNOVA (The Swedish Governmental Agency for Innovation Systems – NanobioIT program, project #22578-2) and the EU FP6 STREP FuSyMEM are gratefully acknowledged for financial support.

References

[1] C.D. Heyes, A.Y. Kobitski, E.V. Amirgoulova, G.U. Nienhaus, J. Phys. Chem. B 108 (2004) 13387–13394.
[2] L.D. Unsworth, H. Sheardown, J.L. Brash, Langmuir 21 (2005) 1036–1041.
[3] P. Harder, M. Grunze, R. Dahin, G.M. Whitesides, P.E. Laibinis, J. Phys. Chem. B 102 (1998) 426–436.
[4] H. Chen, X. Hu, Y. Zhang, D. Li, Z. Wu, T. Zhang, Coll. Surf. B: Biointerfaces 61 (2008) 237–243.
[5] E.K. Schmidt, T. Liebermann, M. Kreiter, A. Jonczyk, R. Naumann, A. Offenhäusser, E. Neumann, A. Kukol, A. Maelicke, W. Knoll, Biosens. Bioelectr. 13 (1998) 585–591.
[6] L. He, J.W.F. Robertson, J. Li, I. Karcher, S.M. Schiller, W. Knoll, R. Naumann, Langmuir 21 (2005) 11666–11672.
[7] S.M. Schiller, R. Naumann, K. Lovejoy, H. Kunz, W. Knoll, Angew. Chem. Int. Ed. 42 (2003) 208–211.
[8] I.K. Vockenroth, P.P. Atanasova, J.R. Long, A.T.A. Jenkins, W. Knoll, I. Köper, Biochim. Biophys. Acta (BBA): Biomembr. 1768 (2007) 1114–1120.
[9] A. Erbe, R.J. Bushby, S.D. Evans, L.J.C. Jeuken, J. Phys. Chem. B 111 (2007) 3515–3524.
[10] I.K. Vockenroth, P.P. Atanasova, A.T.A. Jenkins, I. Koper, Langmuir 24 (2008) 496–502.
[11] L. Becucci, M. Innocenti, E. Salvietti, A. Rindi, I. Pasquini, M. Vassalli, M.L. Foresti, R. Guidelli, Electrochim. Acta 53 (2008) 6372–6379.
[12] J.C. Munro, C.W. Frank, Langmuir 20 (2004) 10567–10575.
[13] G. Elender, M. Kfihner, E. Sackmann, Biosens. Bioelectr. 11 (1996) 565–577.
[14] A. Berquand, P.-E. Mazeran, J. Pantigny, V. Proux-Delrouyre, J.M. Laval, C. Bourdillon, Langmuir 19 (2003) 1700–1707.
[15] C. Elie-Caille, O. Fliniaux, J. Pantigny, J.-C. Mazière, C. Bourdillon, Langmuir 21 (2005) 4661–4668.
[16] S.B. Lei, R. Tero, N. Misawa, S. Yamamura, L.J. Wan, T. Urisu, Chem. Phys. Lett. 429 (2006) 244–249.
[17] F. Giess, M.G. Friedrich, J. Heberle, R.L. Naumann, W. Knoll, Biophys. J. 87 (2004) 3213–3220.
[18] C. Rossi, J. Chopineau, Eur. Biophy. J. 36 (2007) 955–965.
[19] C. Boozer, Q. Yu, S. Chen, C.-Y. Lee, J. Homola, S.S. Yee, S. Jiang, Sens. Actuators B: Chem. 90 (2003) 22–30.
[20] B. Ge, F. Lisdat, Anal. Chim. Acta 454 (2002) 53–64.
[21] E. Ostuni, L. Yan, G.M. Whitesides, Coll. Surf. B: Biointerfaces 15 (1999) 3–30.
[22] G.M. Whitesides, P.E. Laibinis, Langmuir 6 (1990) 87–96.
[23] P. Wessman, A.A. Strömstedt, M. Malmsten, K. Edwards, Biophys. J. 95 (2008) 4324–4336.
[24] B.L. Frey, R.M. Corn, Anal. Chem. 68 (1996) 3187–3193.
[25] A. Kunze, S. Svedhem, B. Kasemo, Langmuir 25 (2009) 5146–5158.
[26] J.H. Scofield, J. Electron. Spectrosc. Relat. Phenom. 8 (1976) 129–137.
[27] F. Höök, B. Kasemo, T. Nylander, C. Fant, K. Sott, H. Elwing, Anal. Chem. 73 (2001) 5796–5804.
[28] M. Rodahl, F. Höök, B. Kasemo, Anal. Chem. 68 (1996) 2219–2227.
[29] J. Lahiri, L. Isaacs, J. Tien, G.M. Whitesides, Anal. Chem. 71 (1999) 777–790.
[30] R. Valiokas, S. Svedhem, C.T. Svensson, B. Liedberg, Langmuir 15 (1999) 3390–3394.
[31] S.-J. Xiao, S. Brunner, M. Wieland, J. Phys. Chem. B 108 (2004) 16508–16517.
[32] P.E. Laibinis, C. Bain, G.M. Whitesides, J. Phys. Chem. B 95 (1991) 7017–7021.
[33] M.D. Porter, T.B. Bright, D.L. Allara, C.E.D. Chidsey, J. Am. Chem. Soc. 109 (1987) 3559–3568.
[34] P. Harder, M. Grunze, R. Dahint, G.M. Whitesides, P.E. Laibinis, J. Phys. Chem. B 102 (1998) 426–436.
[35] S. Svedhem, C.-A. Hollander, J. Shi, P. Konradsson, B. Liedberg, S.C.T. Svensson, J. Org. Chem. 66 (2001) 4494–4503.
[36] B. Pignataro, C. Steinem, H.-J. Galla, H. Fuchs, A. Janshoff, Biophys. J. 78 (2000) 487–498.
[37] L.H. Dubois, B.R. Zegarski, R.G. Nuzzo, J. Chem. Phys. 1 (1993) 678–688.
[38] P.E. Laibinis, G.M. Whitesides, D.L. Allara, Y.-T. Tao, A.N. Parikh, R.G. Nuzzo, J. Am. Chem. Soc. 113 (1991) 7152–7167.
[39] L. Bertilsson, B. Liedberg, Langmuir 9 (1993) 141–149.
[40] S.J. Stranick, A.N. Parikh, Y.T. Tao, D.L. Allara, P.S. Weiss, J. Phys. Chem. 98 (1994) 7636–7646.
[41] V.H. Perez-Luna, M.J. O'Brien, K.A. Opperman, P.D. Hampton, G.P. Lopez, L.A. Klumb, P.S. Stayton, J. Am. Chem. Soc. 121 (1999) 6469–6478.
[42] F. Frederix, K. Bonroy, W. Laureyn, G. Reekmans, A. Campitelli, W. Dehaen, G. Maes, Langmuir 19 (2003) 4351–4357.
[43] M.M.L.M. Vareiro, J. Liu, W. Knoll, K. Zak, D. Williams, A.T.A. Jenkins, Anal. Chem. 77 (2005) 2426–2431.
[44] R.L.C. Wang, H.J. Kreuzer, M. Grunze, J. Phys. Chem. B 101 (1997) 9767–9773.
[45] N.-J. Cho, S.-J. Cho, K.H. Cheong, J.S. Glenn, C.W. Frank, J. Am. Chem. Soc. 129 (2007) 10050–10051.
[46] N.-J. Cho, G. Wang, M. Edvardsson, J.S. Glenn, F. Hook, C.W. Frank, Anal. Chem. 81 (2009) 4752–4761.
[47] V. Agmo Hernandez, F. Scholz, Isr. J. Chem. 48 (2008) 169–184.
[48] E. Briand, M. Zäch, S. Svedhem, B. Kasemo, S. Petronis, Analyst (2010), doi:10.1039/b918288h.